The Aeronautical Journal (2026), 1–17
doi:10.1017/aer.2026.10227

RESEARCH ARTICLE

A collaborative navigation method based on a delay-aware factor graph

Hongru Wang[1,2] and Tongen Fang[1,2]

[1]College of Information and Communication Engineering, Harbin Engineering University, Harbin, 150001, China
[2]Key Laboratory of Advanced Ship Communication and Information Technology, Harbin Engineering University, Harbin, 150001, China
Corresponding author: Tongen Fang; Email: 18135074816@163.com

Received: 17 October 2025 UTC; **Revised:** 23 July 2026 UTC; **Accepted:** 28 July 2026 UTC

Keywords: communication delay; cooperative navigation; distributed optimisation; factor graph; information fusion

Abstract

Aiming at the problem of degradation in navigation accuracy caused by communication delay during cooperative interaction of unmanned aerial vehicle (UAV) formations, a distributed cooperative navigation algorithm based on a delay-aware factor graph is proposed. First, a factor graph model is constructed based on the measurement equations of each sensor. Subsequently, considering the mechanism of ultra-wideband (UWB) transmission delay, a delay factor is formulated and introduced into the factor graph to enable joint estimation with the UAV state. During the initialisation of the factor graph, a prior delay estimate is introduced as an initialisation factor. In order to reduce computational redundancy, a sliding window strategy combined with marginalisation is employed. Furthermore, an adaptive momentum accelerated gradient descent (AMAGD) algorithm is designed to optimise the step size for delay updates. Finally, the global state optimal solution of the delay factor graph is obtained through a message iteration algorithm. The simulation results show that the proposed method can effectively compensate for the loss of accuracy caused by communication delay and improve the positioning accuracy.

Nomenclature

UAV	unmanned aerial vehicle
$\boldsymbol{x}_i^k$	navigation state of UAV i at time t_k
$\delta\boldsymbol{p}$	position error
$\delta\boldsymbol{v}$	velocity error
$\boldsymbol{P}(\boldsymbol{X}^k\|\boldsymbol{Z}^k)$	joint probability density of all state variables and measurements
$\boldsymbol{d}_a$	accelerometer zero bias
$\boldsymbol{d}_g$	gyroscope zero bias
$\boldsymbol{X}_{MAP}^k$	maximum a posteriori estimates of state variables
$\boldsymbol{Z}^k$	all measurements received by the UAV formation at moment k
$\boldsymbol{g}_n$	gravity vector
$\delta\boldsymbol{t}$	communication delay value
$p(x, y)$	joint probability density function

Greek symbol

ψ	attitude
Σ_i	covariance matrix
Λ	information matrix
λ_i	learning rate

© The Author(s), 2026. Published by Cambridge University Press on behalf of Royal Aeronautical Society.

https://doi.org/10.1017/aer.2026.10227 Published online by Cambridge University Press

1.0 Introduction

With the rapid development of unmanned aerial vehicle (UAV) technology and related industries, UAVs are playing an increasingly important role in military and civilian fields due to their small size, low cost and flexibility [1–3]. At the same time, with the increasing diversification and complexity of the tasks performed by UAVs, the limited capability of a single UAV cannot meet the demand, so the development of UAV formation-related technologies has received extensive attention [4, 5]. High-precision navigation and positioning information are crucial for formation technology, which is an important guarantee for UAV formation to achieve precise control, trajectory planning and mission coordination [6]. However, due to factors such as limited on-board computational power, limited bandwidth resources and flight environment interference, communication between UAVs will inevitably be affected by time lag [7]. The communication time lag will lead to the decrease of the estimation accuracy of the cooperative navigation system and the loss or confusion of the measurement information.

To address the problem of communication delays in cooperative navigation systems, conventional approaches include ignoring communication delay, filter recalculation, state augmentation and fixed lag smoothing [8–13]. If the communication time lag is directly ignored, although it can simplify the calculation process, it will lead to sub-optimal state estimation or even divergence. Filter recalculation corrects the time lag data through reverse iteration. Although it can improve the estimation accuracy, the computational complexity grows nonlinearly with the increase of delay duration. The state vector is expanded by the state augmentation method, but the amount of calculation will increase sharply with the increase of dimensions. Although the fixed lag smoothing method can suppress the time lag error, it is difficult to deal with sudden and large delays.

Aiming at the problem of communication time lag processing in cooperative navigation, scholars have proposed a variety of effective improvement methods in recent years, particularly in the domain of underwater vehicles where delays are prominent. Reference [14] proposes an improved error estimation algorithm to address the communication delay problem in autonomous underwater vehicle (AUV) cooperative navigation. In this method, the time delay of underwater acoustic communication is modeled as a measurement deviation, and the delayed measurement information is reconstructed as the equivalent observation value at the current moment and input into the navigation system, which effectively suppresses the positioning deviation caused by the time delay. However, it depends on AUV clock synchronisation and does not solve the problem of noise mutation in dynamic environment. Reference [15] proposes two collaborative positioning algorithms, namely information sequential arrival and information out of sequence arrival, based on the extended Kalman filter framework. These algorithms improve the accuracy of cooperative positioning under communication delay conditions. However, due to the long sampling period, the real-time performance is limited, and the dynamic error compensation ability is insufficient; it is difficult to adapt to the complex formation coordination requirements. In reference [16], a buffer-based delay compensation method is proposed. This method effectively alleviates the problem of communication delay through a block storage mechanism and dynamic weight allocation strategy, but the method has a high demand for storage space. Reference [17] designed a Gaussian prediction model to forecast the current state of an AUV using historical data. It also proposed a backstepping sliding-mode formation control method based on leader-following, effectively compensating for data unreliability caused by acoustic communication delays. Reference [18] proposes a communication delay compensation method based on measurement information reconstruction under the framework of factor graph. The method reconstructs the distance measurement information of the master and slave AUVs during the delay period and iteratively passes it through the factor graph to compensate for communication delay errors. However, this method assumes that the position of the master AUV does not change during the delay period, and its error compensation capability is insufficient in dynamic scenarios.

Recently, the problem of communication delay in UAV formations has also attracted significant attention from researchers. Reference [19] analysed the influence of communication delay on flight stability and estimated the acceptable time-delay limits for positioning missions. Reference [20] designed a position prediction algorithm to actively compensate for communication delays in fixed-wing UAVs and verified the formation stability through hardware-in-the-loop experiments. Reference [21] proposed a

https://doi.org/10.1017/aer.2026.10227 Published online by Cambridge University Press

cooperative longitudinal guidance strategy, which effectively mitigates the impact of inter-UAV communication delay while ensuring formation integrity. Reference [22] proposed a Kalman-fused belief rule base (BRB) model that handles asynchronous data through state prediction and retrospective correction, guaranteeing the reliability of cooperative performance assessment. However, while these works address the delay problem to some extent, they primarily treat delay as a nuisance parameter to be compensated. Constrained by the sequential update mechanism of traditional filtering methods, it is challenging for existing approaches to utilise asynchronous measurements for the effective correction of historical trajectories. In contrast, the factor graph framework transforms the navigation problem into a global optimisation problem, which can ensure higher spatiotemporal consistency through joint estimation. Therefore, this paper proposes a distributed cooperative navigation algorithm based on a delay-aware factor graph (DDFG). The main contributions of this article are summarised as follows:

1. A novel DDFG framework is established by introducing dedicated time delay compensation factor nodes. This framework integrates inertial measurement unit (IMU) pre-integration factors, global navigation satellite system (GNSS) observation factors, and ultra-wideband (UWB) ranging factors into a probabilistic graphical model, enabling the flexible fusion of heterogeneous and asynchronous measurement information.
2. A joint estimation mechanism for stochastic delays and UAV states is proposed. By modeling the random communication delay as an optimised parameter of a Gaussian distribution, the algorithm achieves a globally optimal solution under space-time consistency constraints through nonlinear least squares optimisation.
3. A sliding window marginalisation strategy combined with an adaptive momentum-accelerated gradient descent (AMAGD) algorithm is designed. The sliding window mechanism dynamically retains the nearest N sets of state observations to maintain real-time performance, while the AMAGD algorithm optimises the iteration step size to facilitate the convergence of delay estimation.

The remainder of this paper is organised as follows. Section 2 details the proposed methodology, including the construction of the factor graph model, the formulation of the delay factor graph and the design of the sliding window strategy and the AMAGD algorithm. Section 3 presents the simulation experiments and analyses the results to validate the effectiveness of the proposed method. Finally, Section 4 concludes the paper.

2.0 Method

2.1 Distributed cooperative navigation algorithm based on factor graph

A factor graph is a bipartite probabilistic graphical model used to express the joint probability distribution of random variables [23–25] $F = (\boldsymbol{U}, \boldsymbol{V}, \boldsymbol{E})$. In the factor graph framework [26], the factor node $f_i \in \boldsymbol{U}$, the variable node $\boldsymbol{x}_j \in \boldsymbol{V}$, and the edge $e_{ij} \in \boldsymbol{E}$ always exist between the factor node and the variable node. The resulting factor graph can be defined as a decomposition of the function $f(X)$: $f(\boldsymbol{X}) = \prod_i f_i(\boldsymbol{x}_i)$, where $\boldsymbol{X}$ is the set of all variable nodes associated with the variable node $\mathbf{x}_i$. The factor $f_i(\boldsymbol{x}_i)$ is usually defined as an error function $f_i(\boldsymbol{x}_i) = d(err(\boldsymbol{x}_i, \boldsymbol{z}_i))$, $\boldsymbol{d}(\cdot)$ is the cost function and $\boldsymbol{z}_i$ is the actual measured value.

The information fusion problem for UAV formation cooperative navigation is formulated within a factor graph framework, and the variable node $\boldsymbol{x}_i^k$ is used to represent the navigation state of UAV i at the moment of t_k:

$$\mathbf{x}_i^k = [\,\delta\boldsymbol{p} \quad \delta\boldsymbol{v} \quad \psi \quad \boldsymbol{d}_a \quad \boldsymbol{d}_g\,]^T \tag{1}$$

where $\delta\boldsymbol{p}$ is the position error, $\delta\boldsymbol{v}$ is the velocity error, ψ denotes the attitude, $\boldsymbol{d}_a$ is the acceleration zero bias and $\boldsymbol{d}_g$ is the gyroscope zero bias. Therefore, the navigation state set of UAV formation $\boldsymbol{C}$ at t_k is defined as $\boldsymbol{X}^k = \{\boldsymbol{x}_i^k | i \in C\}$.

https://doi.org/10.1017/aer.2026.10227 Published online by Cambridge University Press

Let $z_{i,k-1}^{IMU}$ represent all measurement data received by the IMU of UAV i from time t_{k-1} to t_k, $z_{i,k}^{UWB}$ represent all UWB ranging measurements received by UAV i at time t_k, and $\mathbf{z}_{i,k}^{GNSS}$ represent all GNSS measurements received by UAV i at time t_k. Therefore, the set of all measured values received by the UAV formation $\boldsymbol{C}$ at t_k can be defined as: $\boldsymbol{Z}^k = \left\{ z_{i,k-1}^{IMU}, z_{i,k}^{UWB}, z_{i,k}^{GNSS} | i \in C \right\}$. The maximum a posteriori estimation of the state variable is expressed as:

$$\boldsymbol{X}_{MAP}^k = \arg\max_{\boldsymbol{X}^k} \boldsymbol{P}\left(\boldsymbol{X}^k | \boldsymbol{Z}^k\right) \tag{2}$$

The resulting joint probability density of all state variables and measurements can be decomposed as [27]:

$$\boldsymbol{P}(\boldsymbol{X}^k | \boldsymbol{Z}^k) = \boldsymbol{P}\left(\boldsymbol{X}_0\right) \prod_{i=1}^{k} P\left(\boldsymbol{x}_i | \boldsymbol{x}_{i-1}, z_{i-1}^{IMU}\right) \prod_{i=1}^{k} \boldsymbol{P}\left(z_i^{GNSS} | \boldsymbol{x}^i\right) \prod_{t=1}^{k} \boldsymbol{P}\left(z_i^{UWB} | \boldsymbol{x}_i^t, \boldsymbol{x}_j^t\right) \tag{3}$$

where $P\left(\boldsymbol{X}_0\right)$ denotes the prior information about the initial state of all variables, $P\left(\boldsymbol{x}_i | \, \boldsymbol{x}_{i-1}, z_{i-1}^{IMU}\right)$ denotes the state probability density function of IMU, $P\left(z_i^{GNSS} | \boldsymbol{x}^i\right)$ and $P\left(z_i^{UWB} | \boldsymbol{x}_i^t, \boldsymbol{x}_j^t\right)$ denote the conditional probability density functions of GNSS and UWB, respectively.

In the factorisation of the joint probability density function $P\left(\boldsymbol{X}^k | \boldsymbol{Z}^k\right)$, each factor represents an independent term, so the joint probability density function can be decomposed as:

$$\boldsymbol{P}\left(\boldsymbol{X}^k | \boldsymbol{Z}^k\right) \propto \prod_i f_i\left(\boldsymbol{X}_i^k\right), \boldsymbol{X}_i^k \in \boldsymbol{X}^k \tag{4}$$

In this paper, it is assumed that the noise obeys a Gaussian distribution [28] and the factor nodes can be described as:

$$f_i\left(\boldsymbol{x}_i\right) = d\left(err\left(x_i^k, z^k\right)\right) = \exp\left\{-\frac{1}{2}\left|\left|h_i\left(\boldsymbol{x}_i^k\right) - \mathbf{z}^k\right|\right|_{\Sigma_i}^2\right\} \tag{5}$$

where $||\cdot||_{\Sigma}^2$ represents the squared Mahalanobis distance, Σ_i represents the process noise covariance matrix and $h_i\left(\boldsymbol{x}\right)$ is the nonlinear measure function. The maximum a posteriori estimation problem can then be transformed into a nonlinear least-squares problem [29].

$$\boldsymbol{X}_{MAP}^k = \arg\min_{\boldsymbol{X}^k} \sum_i \left|\left|h_i\left(\mathbf{x}_i^k\right) - \boldsymbol{z}^k\right|\right|_{\Sigma_i}^2 \tag{6}$$

In the distributed UAV formation cooperative navigation process, each UAV only processes its own IMU and GNSS information as well as the UWB ranging information that satisfies the current constraints, and the position optimisation of the UAVs is achieved through message iteration. The factor graph optimisation function can be expressed as:

$$\arg\min \sum_k \|\mathbf{r}_{IMU}^k(\mathbf{X}_k, \mathbf{X}_{k+1})\|_{\Sigma_{IMU}}^2 + \sum_k \|\mathbf{r}_{GNSS}^k(\mathbf{X}_k)\|_{\Sigma_{GNSS}}^2 + \sum_k \left(\|\mathbf{r}_{ij}^{k,UWB}(\mathbf{X}_i^k, \mathbf{X}_j^k)\|_{\Sigma_d}^2\right) \tag{7}$$

where $\boldsymbol{r}$ represents the residual. Using Taylor's formula to linearise the above equation, it is transformed into a least squares problem. The specific simplification process is referred to in reference [30], and the optimal estimation value is solved by the Gauss-Newton method.

Here, taking three UAVs as an example, the distributed UAV formation cooperative navigation factor graph structure is shown in Fig. 1.

In this paper, each UAV is equipped with a suite of sensors, including an IMU, a GNSS receiver and a UWB ranging module. The following is a simple derivation of the factor formula of the above sensor measurement model.

2.1.1 IMU factor node

The INS produces high-rate measurements due to its high output frequency and different sampling frequency from other sensors. In order to achieve plug-and-play for each sensor in the factor graph while

https://doi.org/10.1017/aer.2026.10227 Published online by Cambridge University Press

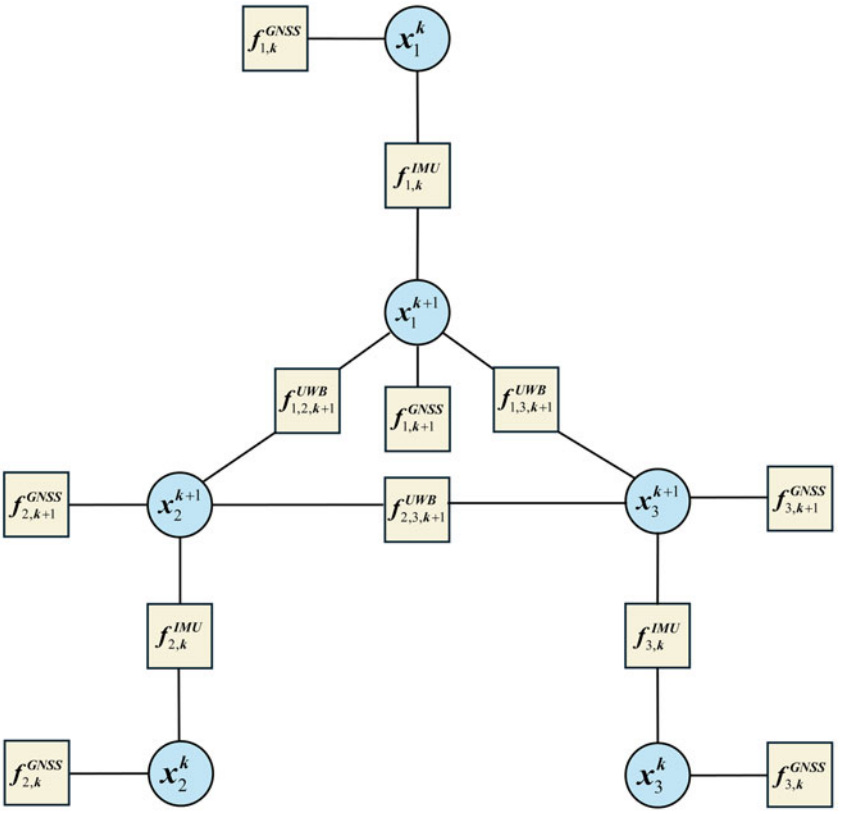


Figure 1. *UAV formation cooperative navigation factor graph model.*

reducing the update frequency of the factor graph, this paper uses pre-integration to construct factor nodes.

Let one update cycle of the INS pre-integration be $t_k \sim t_{k+1}$, and the position, velocity and attitude increments during the cycle be:

$$\begin{cases} \Delta \mathbf{p}_{t_k}^{t_{k+1}} = \int \int_{t_k}^{t_{k+1}} \mathbf{C}_{b_{t_k}}^{b_t} \left(\mathbf{d}_t^b - \nabla \mathbf{d}_a \right) dt^2 \\ \Delta \mathbf{v}_{t_k}^{t_{k+1}} = \int_{t_k}^{t_{k+1}} \mathbf{C}_{b_{t_k}}^{b_t} \left(\mathbf{d}_t^b - \nabla \mathbf{d}_a \right) dt \\ \Delta \psi_{t_k}^{t_{k+1}} = \int_{t_k}^{t_{k+1}} \mathbf{E}_{b_{t_k}}^{b_t} \left(\mathbf{g}_t^b - \nabla \mathbf{d}_g \right) dt \end{cases} \tag{8}$$

where $\boldsymbol{C}_{b_{t_k}}^{b_t}$ and $\boldsymbol{E}_{b_{t_k}}^{b_t}$ denote the rotation matrix and rotation rate matrix of the carrier coordinate system at time t relative to the start moment t_k, respectively. $\boldsymbol{d}_t^b$ and $\mathbf{g}_t^b$ represent the accelerometer and gyroscope measurements at moment t, while $\nabla \boldsymbol{d}_a$ and $\nabla \boldsymbol{d}_g$ denote their corresponding biases. By combining these incremental measurements with the navigation state at t_k, the state at t_{k+1} is updated as follows:

$$\begin{cases} \boldsymbol{p}_{t_{k+1}}^n = \boldsymbol{p}_{t_k}^n + (t_{k+1} - t_k) \boldsymbol{v}_{t_k}^n + \frac{1}{2} (t_{k+1} - t_k)^2 \mathbf{g}^n + \boldsymbol{C}_{b_{t_k}}^n \Delta \boldsymbol{p}_{t_k}^{t_{k+1}} \\ \boldsymbol{v}_{t_{k+1}}^n = \boldsymbol{v}_{t_k}^n + (t_{k+1} - t_k) \mathbf{g}^n + \boldsymbol{C}_{b_{t_k}}^n \Delta \boldsymbol{v}_{t_k}^{t_{k+1}} \\ \psi_{t_{k+1}}^n = \psi_{t_k}^n + \boldsymbol{C}_{b_{t_k}}^n \Delta \psi_{t_k}^{t_{k+1}} \end{cases} \tag{9}$$

where $\mathbf{g}^n$ is the gravity vector, $\boldsymbol{C}_{b_{t_k}}^n$ is the rotation matrix of the navigation coordinate system relative to the carrier coordinate system at the moment of t_k, from which we get the information of position, velocity and attitude under the navigation coordinate system at the moment of t_{k+1}.

Let UAV i receive the measurement information $z_{i,t_k}^{IMU} = \{\boldsymbol{d}^b, \mathbf{g}^b\}$, and according to the INS pre-integration process, the estimated value of the navigation state of UAV i at the moment t_{k+1} moment

https://doi.org/10.1017/aer.2026.10227 Published online by Cambridge University Press

status update value:

$$\boldsymbol{x}_i^{t_{k+1}} = h\left(\boldsymbol{x}_i^{t_k}, z_{i,t_k}^{IMU}, t_k\right) \tag{10}$$

where $\boldsymbol{x}_i^{t_k}$ is the position, velocity and attitude information of the INS carried by UAV i at the t_k moment. Let $\alpha_i^{t_k}$ be the deviation correction value of the accelerometer and gyroscope at t_k, and the predicted value of INS navigation state at t_{k+1} is obtained by $\hat{x}_i^{t_{k+1}} = h(x_i^{t_k}, \alpha_i^{t_k}, z_{i,t_k}^{IMU})$. Thus, the IMU factor node is defined as:

$$\boldsymbol{f}_{i,t_k}^{IMU}\left(\boldsymbol{x}_i^{t_k}, \boldsymbol{x}_i^{t_{k+1}}\right) = d\left(\hat{\boldsymbol{x}}_i^{t_{k+1}} - \boldsymbol{x}_i^{t_{k+1}}\right) = \exp\left(-\frac{1}{2}\left|\left|\hat{\boldsymbol{x}}_i^{t_{k+1}} - \boldsymbol{x}_i^{t_{k+1}}\right|\right|_{\Sigma_{IMU}}^2\right) \tag{11}$$

The IMU residual model can be expressed as:

$$\boldsymbol{r}_{IMU}^k\left(\boldsymbol{X}_k, \boldsymbol{X}_{k+1}\right) \propto \hat{\boldsymbol{x}}_i^{t_{k+1}} - \boldsymbol{x}_i^{t_{k+1}} \tag{12}$$

2.1.2 UWB factor node

The distance between UAV i and UAV j is modelled as:

$$\boldsymbol{d}_{i,j}^{UWB} = \boldsymbol{d}_{i,j} + \boldsymbol{n}_{UWB} \tag{13}$$

where $\boldsymbol{d}_{i,j}$ is the true distance between the two UAVs, $\boldsymbol{n}_{UWB}$ is the UWB ranging noise, and the distance observation function $h(\boldsymbol{x}_i, \boldsymbol{x}_j)$ between UAVs can be expressed as:

$$h(\boldsymbol{x}_i, \boldsymbol{x}_j) = \sqrt{\boldsymbol{x}_i \boldsymbol{x}_j^T} = \sqrt{\left(\boldsymbol{x}_i^e - \boldsymbol{x}_j^e\right)^2 + \left(\boldsymbol{x}_i^n - \boldsymbol{x}_j^n\right)^2 + \left(\boldsymbol{x}_i^u - \boldsymbol{x}_j^u\right)^2} \tag{14}$$

Thus, the UWB ranging factor is defined as:

$$\boldsymbol{f}_{i,j}^{UWB}(\boldsymbol{x}_i, \boldsymbol{x}_j) = \boldsymbol{d}\left(\boldsymbol{d}_{i,j}^{UWB} - h(\boldsymbol{x}_i, \boldsymbol{x}_j)\right) = \exp\left(-\frac{1}{2}\left|\left|\boldsymbol{d}_{i,j}^{UWB} - h(\boldsymbol{x}_i, \boldsymbol{x}_j)\right|\right|_{\Sigma_d}^2\right) \tag{15}$$

The UWB ranging factor residual model is expressed as:

$$\boldsymbol{r}_{ij}^{k,WB} \propto \boldsymbol{d}_{i,j}^{UWB} - h(\boldsymbol{x}_i, \boldsymbol{x}_j) \tag{16}$$

2.1.3 GNSS factor node

The GNSS measurement equation can generally be modelled as:

$$z_i^{GNSS} = h^{GNSS}\left(\boldsymbol{x}_i\right) + \eta_{GNSS} \tag{17}$$

where $h^{GNSS}(\bullet)$ denotes the relationship between the carrier's current navigation state and the GNSS measurements z_i^{GNSS}, and η_{GNSS} is the GNSS measurement noise. The GNSS factor of UAV i at the moment t_k is defined as:

$$\boldsymbol{f}_{i,t_k}^{GNSS}\left(\boldsymbol{x}_i^{t_k}\right) = d\left(z_{i,t_k}^{GNSS} - h^{GNSS}\left(\boldsymbol{x}_i^{t_k}\right)\right) = \exp\left(-\frac{1}{2}\left|\left|z_{i,t_k}^{GNSS} - h^{GNSS}\left(\boldsymbol{x}_i^{t_k}\right)\right|\right|_{\Sigma_{GNSS}}^2\right) \tag{18}$$

The GNSS factor residual model can be expressed as:

$$\boldsymbol{r}_{\mathrm{GNSS}}^k\left(\boldsymbol{X}_k\right) \propto \boldsymbol{z}_{i,t_k}^{\mathrm{GNSS}} - h^{\mathrm{GNSS}}\left(\boldsymbol{x}_i^{t_k}\right) \tag{19}$$

2.2 Delay factor graph model

The transmission delay of UWB communication technology is mainly composed of fixed delay, propagation delay and random delay. Fixed delay mainly includes system processing delay and wireless network queuing delay in a multi-user environment. Propagation delay is usually proportional to the distance. Among them, the random delay is caused by multiple factors, such as the multipath effect and non-line-of-sight (NLOS) propagation in complex environments. Thus, the transmission delay model of UWB communication is established:

$$\delta t = \Delta T + \frac{\boldsymbol{z}_k^i}{c} + t_\eta \tag{20}$$

https://doi.org/10.1017/aer.2026.10227 Published online by Cambridge University Press

where ΔT is the communication fixed delay, t_η is the random communication delay obeying a Gaussian distribution with mean 0 and variance σ^2. z_k^i expresses the inter-UAV communication distance and c is the speed of light.

The transmission distance of UWB communication is within 1km, and the communication delay is generally less than 1s. Thus, the relevant propagation delay z_k^i/c is on the order of microseconds, and the communication transmission delay model can be simplified as:

$$\delta t \approx \Delta T + t_\eta, \quad \delta t \sim \mathrm{N}(\Delta T, \sigma^2) \tag{21}$$

The short-term flight trajectory of UAV formation can be approximated as linear motion, so the position and ranging information of UAV i and UAV j can be expressed as:

$$\begin{cases} \boldsymbol{p}_i^k \approx \boldsymbol{p}_i^{k-\delta t} + \boldsymbol{v}_i^{k-\delta t}\delta t + \frac{1}{2}a_i^{k-\delta t}\delta t^2 \\ \boldsymbol{p}_j^k \approx \boldsymbol{p}_j^{k-\delta t} + \boldsymbol{v}_j^{k-\delta t}\delta t + \frac{1}{2}a_j^{k-\delta t}\delta t^2 \\ \boldsymbol{d}_{ij} = \left|\left|\boldsymbol{p}_i^k - \boldsymbol{p}_j^k\right|\right| \end{cases} \tag{22}$$

Let UAV i receive the measurement information of UAV j at k moments, but the information corresponds to the measurement information of UAV j at $k-\delta t$ moments. Let the state of UAV j at the moment of $k-\delta t$ be $\boldsymbol{X}_j^{k-\delta t}$, and use the state transfer model to predict the state of UAV j at the current moment of k to be:

$$\hat{\boldsymbol{X}}_j^k = h\left(\boldsymbol{X}_j^{k-\delta t}, \delta t\right) \tag{23}$$

where $h(\bullet)$ is the state propagation function from $\boldsymbol{X}_j^{k-\delta t}$ to $\boldsymbol{X}_j^k$.

Because δt is unknown, it needs to be obtained after factor graph optimisation, the factor requires delayed prior information as a starting term. From Equation (21), the residual squared term of the delayed a priori factor can be expressed as:

$$||\boldsymbol{r}_t^k(\delta t)||_{\Sigma_t}^2 = (\delta t^k - \Delta T)^T \boldsymbol{\Sigma}_t^{-1}(\delta t^k - \Delta T) \tag{24}$$

For the UWB ranging module, let the position information of UAV i at k moments be p_i^k, and the predicted value of the position of UAV j at k moments be $\hat{\boldsymbol{p}}_j^k$, which is obtained from Equation (22). The UWB ranging residual including communication delay is expressed as:

$$\boldsymbol{r}_d = \| \boldsymbol{p}_i^k - \hat{\boldsymbol{p}}_j^k \| - \boldsymbol{d}_{ij,k}^{UWB} \tag{25}$$

where $\boldsymbol{d}_{ij,k}^{UWB}$ is the true distance between UAV i and UAV j at k moments.

The UWB factor considering communication delay is modified to:

$$\boldsymbol{f}^{UWB}\left(\boldsymbol{X}_{ij}^k, \delta t\right) = \exp\left\{-\frac{1}{2}\| \boldsymbol{r}_d \|_{\Sigma_d}^2\right\} \tag{26}$$

where $\boldsymbol{X}_{ij}^k$ denotes the state information of UAV i and UAV j at k moments, and the ranging covariance Σ_d with delay is expressed as:

$$\Sigma_d = \Sigma_{uwb} + \Sigma_t = \Sigma_{uwb} + H\sigma^2 H^T \tag{27}$$

where $\boldsymbol{\Sigma}_{uwb}$ is the UWB's own measurement covariance, and $\boldsymbol{H}$ is the delayed Jacobian matrix:

$$\boldsymbol{H} = \frac{\partial h\left(\boldsymbol{X}_j^{k-\tau}, \delta t\right)}{\partial \delta t} \tag{28}$$

Therefore, the optimisation function of UAV formation cooperative navigation factor graph considering communication delay is expressed as:

$$\begin{aligned} &\arg\min \sum_{\boldsymbol{X},\delta t} \| \boldsymbol{r}_{IMU}^k(\boldsymbol{X}_k, \boldsymbol{X}_{k+1}) \|_{\Sigma_{IMU}}^2 + \sum_k \| \boldsymbol{r}_{GNSS}^k(\boldsymbol{X}_k) \|_{\Sigma_{GNSS}}^2 \\ &+ \sum_k \left(\| \boldsymbol{r}_{ij}^{k,UWB}\left(\boldsymbol{X}_i^k, \boldsymbol{X}_j^{k-\delta t}, \delta t\right) \|_{\Sigma_d}^2 + \| \boldsymbol{r}_t^k(\delta t) \|_{\Sigma_t}^2 \right) \end{aligned} \tag{29}$$

https://doi.org/10.1017/aer.2026.10227 Published online by Cambridge University Press

2.3 Sliding window design

In the process of iterative optimisation, each time the system uploads the measurement value of a sensor, the factor graph will generate a new node. As the number of objective function items increases, the number of rows of the Jacobian matrix will increase, which will seriously increase the computational burden. The sliding window method is used to dynamically retain the recent critical state measurements to limit the scope of optimisation [31], which effectively balances the state estimation accuracy with the computational efficiency and improves the system real-time performance. A sliding window with a width of $N(1 \le N \le l)$ is set, and the UAV solves the factor graph optimisation by combining the previous N sets of sensor observations and state information for the current moment.

Let the set of states and measures in the sliding window at moment k be $Q = \{\boldsymbol{X}_1^k, \boldsymbol{X}_2^k, \cdots, \boldsymbol{X}_n^k, \boldsymbol{Z}_1^k, \boldsymbol{Z}_2^k, \cdots, \boldsymbol{Z}_n^k | n \in N\}$, the joint probability density distribution of the factor graph can be rewritten as:

$$\begin{aligned} \boldsymbol{p}(\boldsymbol{X}^k|Z^k) = \boldsymbol{p}(\boldsymbol{X}^0) \cdot \prod_{k\in N} \boldsymbol{p}(\boldsymbol{x}^k|\boldsymbol{z}^{k-1,IMU}, \boldsymbol{x}^{k-1}) \cdot \\ \prod_{k\in N} \boldsymbol{p}(\boldsymbol{z}^{k,GNSS}|\boldsymbol{x}^k) \cdot \prod_{k\in N} \boldsymbol{p}\left(\boldsymbol{z}^{k,UWB}|\boldsymbol{x}_i^k, \boldsymbol{x}_j^{k-\delta t}\right) \cdot \prod_{k\in N} \boldsymbol{p}\left(\delta t_{ij}^k \middle| \delta t_{ij}^{k-1}\right) \end{aligned} \tag{30}$$

Simply using the sliding window to filter out the state and measurement values at distant times in the past may cause the loss of epoch information, resulting in the non-global optimal solution for the estimated value. The old nodes are removed without loss of calendar element information by the marginalisation operation. Let x be the variable nodes to be filtered, y be the new variable node, the joint probability density can be expressed as $\boldsymbol{p}(\boldsymbol{x}, \boldsymbol{y})$ in the sliding window range, and the probability density $\boldsymbol{p}(\boldsymbol{y})$ of the node y can be obtained by integrating the marginalised node x.

Let the joint probability density $\boldsymbol{p}(\boldsymbol{x}, \boldsymbol{y})$ conform to a Gaussian distribution, chunked in the form of an information vector and an information matrix:

$$\boldsymbol{p}(\boldsymbol{x}, \boldsymbol{y}) = N\left(\boldsymbol{\Lambda}^{-1} \begin{bmatrix} \eta_x \\ \eta_y \end{bmatrix}, \begin{bmatrix} \boldsymbol{\Lambda}_{xx} & \boldsymbol{\Lambda}_{xy} \\ \boldsymbol{\Lambda}_{yx} & \boldsymbol{\Lambda}_{yy} \end{bmatrix}^{-1}\right) \tag{31}$$

Based on the factor graph linearisation process and the Gauss-Newton method, there are:

$$\Lambda \Delta \boldsymbol{X} = \boldsymbol{b} \tag{32}$$

where $\Delta \boldsymbol{X}$ is the state node increment, Λ is the information matrix, $\Lambda = \boldsymbol{J}^T \boldsymbol{J}$, $\boldsymbol{J}$ is the Jacobi matrix, $\boldsymbol{b} = \boldsymbol{J}^T \boldsymbol{r}$, $\boldsymbol{r}$ is the residual term corresponding to factor nodes associated with variable nodes. The matrix is divided into blocks, there are:

$$\begin{bmatrix} \Lambda_{xx} & \Lambda_{xy} \\ \Lambda_{yx} & \Lambda_{yy} \end{bmatrix} \begin{bmatrix} \Delta \boldsymbol{x} \\ \Delta \boldsymbol{y} \end{bmatrix} = \begin{bmatrix} \boldsymbol{b}_x \\ \boldsymbol{b}_y \end{bmatrix} \tag{33}$$

The variable x is eliminated by matrix Schur complement operation, and the following is obtained:

$$\left(\Lambda_{yy} - \Lambda_{yx}\Lambda_{xx}^{-1}\Lambda_{xy}\right)\Delta \boldsymbol{y} = \boldsymbol{b}_y - \Lambda_{yx}\Lambda_{xx}^{-1}\Lambda_{xy} \tag{34}$$

In summary, even if there is no old variable x, the remaining variable y can be solved. And the constraint information of the old variables is retained in the information matrix, set:

$$\begin{cases} \boldsymbol{\Lambda}_y^0 = \boldsymbol{\Lambda}_{yy} - \boldsymbol{\Lambda}_{yx}\boldsymbol{\Lambda}_{xx}^{-1}\boldsymbol{\Lambda}_{xy} \\ \boldsymbol{b}_y^0 = \boldsymbol{b}_y - \boldsymbol{\Lambda}_{yx}\boldsymbol{\Lambda}_{xx}^{-1}\boldsymbol{\Lambda}_{xy} \end{cases} \tag{35}$$

Then the priori information of the remaining variable y can be expressed as:

$$\boldsymbol{p}\left(\boldsymbol{y}^0\right) \propto \exp\left(\left(\boldsymbol{b}_y^0\right)^T \boldsymbol{y} - \boldsymbol{y}^T A_y^0 \boldsymbol{y}\right) \tag{36}$$

https://doi.org/10.1017/aer.2026.10227 Published online by Cambridge University Press

Thus, the final optimised objective function for the factor graph within the sliding window can be obtained:

$$\begin{aligned} X_{MAP}^{k} = \arg\min_{X,\delta t} & \left\| (b^0)^T X_k - X_k^T \Lambda_y^0 X_k \right\|_{\Sigma_0}^2 \\ & + \sum_{k \in N} \left\| r_{IMU}^k (X_k, X_{k+1}) \right\|_{\Sigma_{IMU}}^2 \\ & + \sum_{k \in N} \left\| r_{GNSS}^k (X_k) \right\|_{\Sigma_{GNSS}}^2 \\ & + \sum_{k \in N} \left(\left\| r_{ij}^{k,UWB} (X_i^k, X_j^{k-\delta t}, \delta t) \right\|_{\Sigma_d}^2 + \left\| r_t^k (\delta t) \right\|_{\Sigma_t}^2 \right) \end{aligned} \tag{37}$$

2.4 Delayed estimation of iterative step size optimisation

Considering the real-time performance of the system, the number of message iterations of the factor graph algorithm is limited to 5 times. In order to achieve fast convergence of delay estimates during the limited number of iterations, the AMAGD algorithm is designed by combining historical delay estimates with real-time observation data. By dynamically adjusting the learning rate and introducing the momentum term, the historical gradient information is used to accelerate the convergence. At the same time, combined with the joint determination of ranging error and positioning error, the error is minimised within a limited number of iterations.

According to the cooperative navigation algorithm mentioned in this paper, the communication delay will cause the ranging time to lag behind reality, resulting in ranging error. When the delayed ranging data is used for positioning, it will further lead to the deviation of position estimation, so the ranging and position errors are correlated with the communication delay. The ranging error and position error after each iteration are calculated respectively:

$$\begin{cases} \boldsymbol{e}_{uwb} = \| \boldsymbol{p}_i - \hat{\boldsymbol{p}}_j \left(\delta \hat{t} \right) \| - \boldsymbol{d}_{ij} \\ \boldsymbol{e}_p = \| \hat{\boldsymbol{p}}_i - \boldsymbol{p}_i \| \end{cases} \tag{38}$$

where, $\hat{\boldsymbol{p}}_j \left(\delta \hat{t} \right)$ is the position delay compensation calculated by Equation (22) for this iteration delayed solution $\delta \hat{t}$, $\hat{\boldsymbol{p}}_i$ is the estimated position of this iteration, $\boldsymbol{d}_{ij}$ and $\boldsymbol{p}_i$ are the real distance and the real position, respectively. According to $\boldsymbol{e}_{uwb}$ and $\boldsymbol{e}_p$, the joint loss function can be established as:

$$\boldsymbol{L}(\delta \hat{t}) = \alpha \boldsymbol{e}_{uwb}^2 + \beta \boldsymbol{e}_p^2 + \gamma (\delta \hat{t} - \mu)^2 \tag{39}$$

where α and β are the weights of distance measurement error and positioning error, respectively, and $0 < \beta < \alpha \leq 1$. γ is the delay prior weight ($\gamma = 1/\sigma^2$ for Gaussian distribution).

Calculate the gradient of the loss function with respect to the delay time:

$$\nabla \boldsymbol{L} = 2\alpha \boldsymbol{e}_{uvb} \frac{\partial \boldsymbol{e}_{uvb}}{\partial \delta \hat{t}} + 2\beta \boldsymbol{e}_p \frac{\partial \boldsymbol{e}_p}{\partial \delta \hat{t}} + 2\gamma (\delta \hat{t} - \mu) \tag{40}$$

Among them:

$$\begin{cases} \frac{\partial \boldsymbol{e}_{uwb}}{\partial \delta \hat{t}} = \frac{(\boldsymbol{p}_i - \hat{\boldsymbol{p}}_j)^T}{\| \boldsymbol{p}_i - \hat{\boldsymbol{p}}_j \|} \cdot (\mathbf{v}_j + \mathbf{a}_j \delta \hat{t}) \\ \frac{\partial \mathbf{e}_p}{\partial \delta \hat{t}} = \frac{\partial \boldsymbol{p}_i}{\partial \delta \hat{t}} \cdot \frac{\hat{\boldsymbol{p}}_i - \boldsymbol{p}_i}{\| \hat{\boldsymbol{p}}_i - \boldsymbol{p}_i \|} \end{cases} \tag{41}$$

For a more stable accelerated convergence of the delay estimates, the momentum term $\boldsymbol{m}_k$ is set to denote an exponentially weighted moving average of the historical gradients:

$$\boldsymbol{m}_k = \eta \cdot \boldsymbol{m}_{k-1} + (1 - \eta) \cdot \nabla \boldsymbol{L} \tag{42}$$

where η is the momentum decay rate, usually $0 < \eta < 1$.

https://doi.org/10.1017/aer.2026.10227 Published online by Cambridge University Press

Table 1. *Parameters for each sensor*

Sensor	Parameter	Value
Gyroscope	Random constant/(°)·h^{-1}	0.02
	White noise/(°)·h^{-1}	0.02
	1st-order Markov noise/(°)·h^{-1}	0.02
	Update frequency/Hz	50
Accelerometer	1st-order Markov bias error/g	0.0001
	Update frequency/Hz	50
UWB	Ranging error/m	0.5
	Update frequency/Hz	5

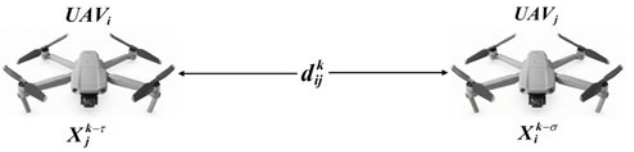


Figure 2. *UAV communication delay diagram.*

The learning rate is set to adaptively adjust the update step size, and the initial learning rate is set to:

$$\lambda_0 = \lambda_b \cdot \frac{|\delta\hat{t} - \mu|}{\sigma} \tag{43}$$

where λ_b is the base learning rate, set to 0.1.

The learning rate parameter is adjusted according to the update trend of the loss function. If the loss decreases in two consecutive iterations, then: $\lambda_k = \min(1.1\lambda_{k-1}, \lambda_{max})$. If the loss value increases, then: $\lambda_k = \max(0.5\lambda_{k-1}, \lambda_{min})$, otherwise it remains unchanged.

In summary, the delay estimation update value is obtained:

$$\delta t_{k+1} = \delta t_k - \lambda_k m_k \tag{44}$$

3.0 Results

3.1 Simulation setup

Simulation experiments were carried out for distributed UAV formation cooperative navigation. The formation consists of three UAVs. Each UAV is equipped with an IMU, Global Positioning System (GPS) and UWB. The sensor parameters were referenced from the open-source navigation website (www.psins.org.cn). The GPS three-axis positioning error is set to [0.2m 0.2m 0.5m], and the detailed data for IMU and UWB are listed in Table 1. In the experiment, other position errors are set to follow a zero-mean Gaussian white noise distribution with a standard deviation of 2m, and the velocity error follows a Gaussian distribution with a standard deviation of 0.1m/s. The sliding window size is set to $N = 15$. The communication delay model and delay topology between UAVs are shown in Figs 2 and 3, respectively. Figure 4 shows the flight trajectory of the three UAVs in the experiment.

The communication delay between UAVs is assumed to follow a Gaussian distribution, and the following conditions are satisfied:

1. In the experiment, six groups of one-way communication delay curves are used to characterise the communication topology characteristics of the UAV formation, as shown in Fig. 5. Specifically, UAV*12*, UAV*13*, UAV*21*, UAV*23*, UAV*31* and UAV*32* are defined, where UAV*ij* denotes the communication delay of the receiving node UAV *j* relative to the transmitting node UAV *i*.

https://doi.org/10.1017/aer.2026.10227 Published online by Cambridge University Press

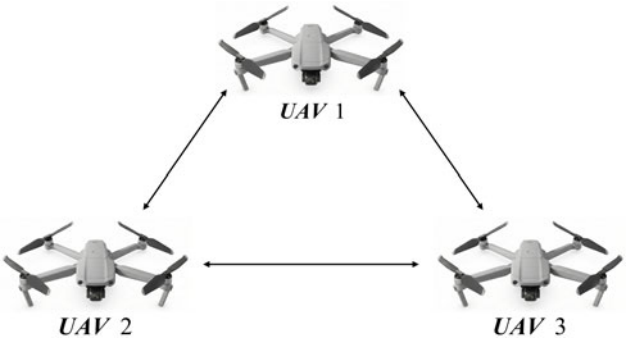


Figure 3. *Distributed time delay topology.*

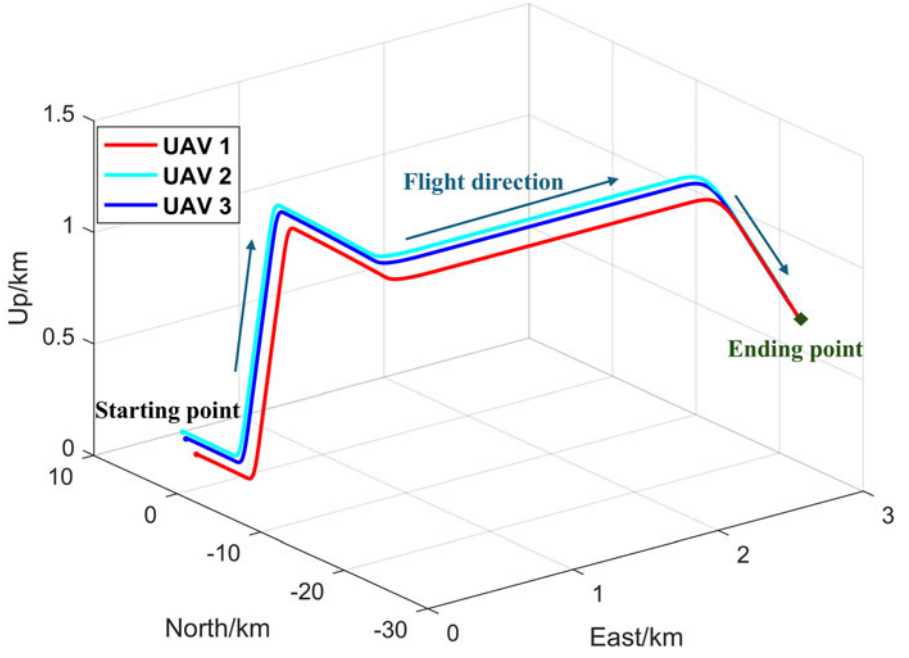


Figure 4. *UAV formation trajectory diagram.*

2. Affected by the wireless channel random noise and multipath interference, the communication link shows significant asymmetric characteristics, and the time lag measurements in different transmission directions between two nodes are statistically different ($\boldsymbol{p} < 0.05$).
3. Under the same hardware configuration and environmental interference conditions, the communication delay between each node pair is assumed to follow an independent and identically distributed Gaussian model with a mean $\Delta T = 0.2\,\mathrm{s}$ and a standard deviation $\sigma = 0.05$. The delay processes of different communication links are considered mutually independent.

3.2 Simulation results and analysis

Based on the simulation conditions described above, trajectory tracking simulations were conducted, and the position and velocity estimation errors were analysed. In order to verify the effectiveness and reliability of the proposed DDFG algorithm, the proposed algorithm is compared with the factor graph cooperative navigation algorithm based on the reconstruction of the measurement information in the

https://doi.org/10.1017/aer.2026.10227 Published online by Cambridge University Press

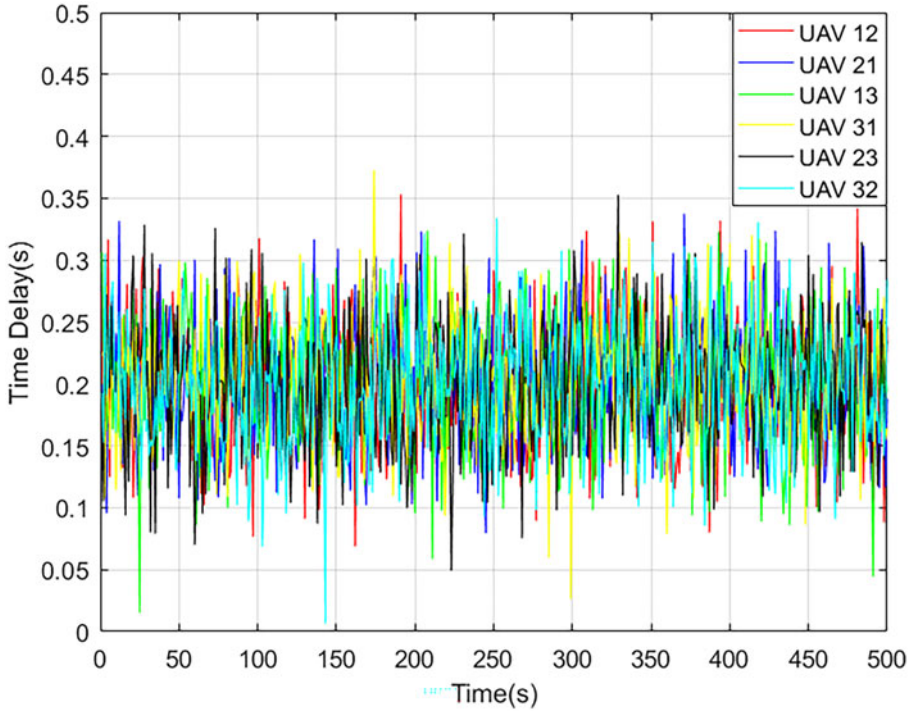


Figure 5. *Simulation diagram of communication delay between UAV formations.*

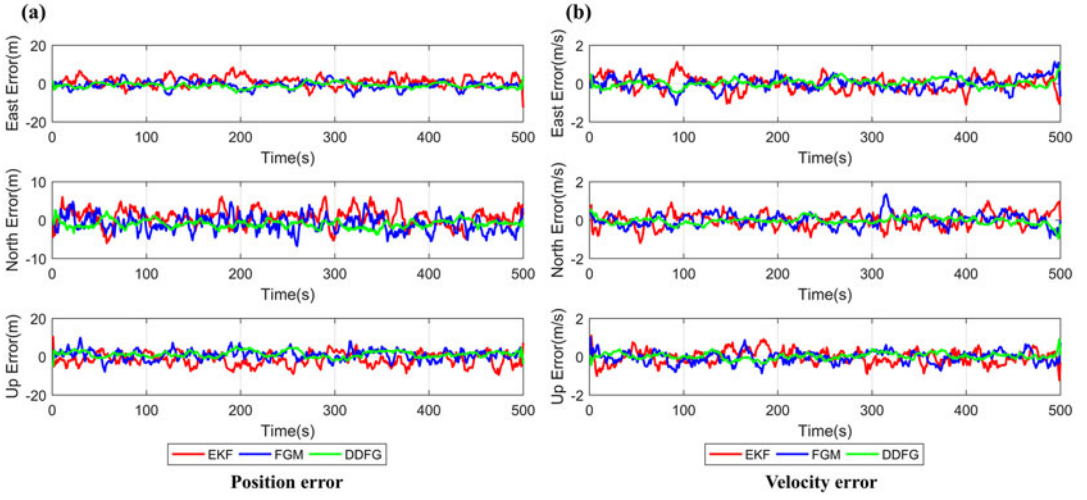


Figure 6. *Comparison of velocity error and position error of UAV 1.*

case of communication delay (FGM) [18], and the distributed extended Kalman filter (DEKF) that takes into account the communication delays [15].

Each UAV is equipped with a high-precision master clock that broadcasts the system clock via UWB links. Synchronisation is achieved through timestamp parsing and clock offset compensation. The system switches to the GNSS timing mode under the stable satellite navigation signal scenario. The simulation results are shown in Figs 6 and 7. Table 2 shows the statistical three-dimensional root mean square

https://doi.org/10.1017/aer.2026.10227 Published online by Cambridge University Press

Table 2. *RMSE comparison of different algorithms*

UAV	Metrics	Algorithm		
		DEKF	**FGM**	**DDFG**
UAV1	Position (m)	4.91 ± 1.15	4.28 ± 0.91	3.17 ± 0.36
	Velocity (m/s)	0.64 ± 0.21	0.54 ± 0.19	0.36 ± 0.08
UAV2	Position (m)	5.11 ± 1.19	4.13 ± 0.88	2.97 ± 0.32
	Velocity (m/s)	0.60 ± 0.19	0.52 ± 0.14	0.34 ± 0.06

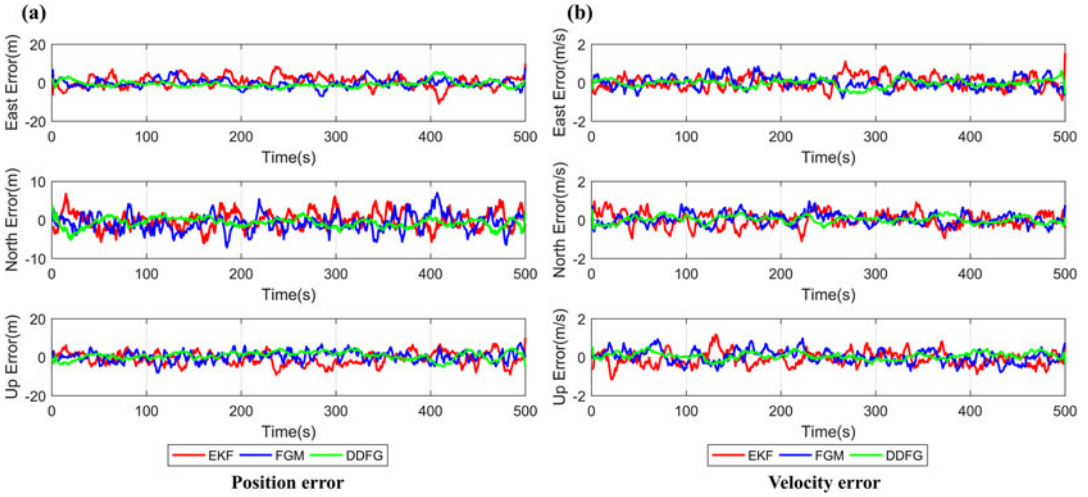


Figure 7. *Comparison of velocity error and position error of UAV 2.*

errors (RMSE, Mean $\pm$ Standard Deviation (SD)) of position and velocity obtained from 100 Monte Carlo runs.

Comparing Figs 6, 7 and Table 2, it can be seen that the proposed DDFG algorithm has the smallest positional error compared to the other two algorithms in the simulation experiments in the presence of communication delays. Compared with FGM and DEKF, the proposed algorithm improves the average position accuracy by 27.01% and 38.66%, respectively. Similarly, the average velocity accuracy is improved by 33.97% and 43.54%, respectively. The proposed algorithm adjusts the delay update step size of the next iteration in each iteration according to the state error value of the last iteration, so that the delay estimation value quickly converges to the actual delay value in a limited number of iterations without sharp peaks. From the delay estimation in Fig. 8, it can be seen that the delay value estimated by this algorithm is close to the actual delay except for the large fluctuation.

To further validate the effectiveness and robustness of the algorithm under different communication conditions, the system fixed delay is set to 0.3s, 0.5s, 0.7s and 0.9s, respectively. For each delay condition, 100 Monte Carlo simulations are carried out to ensure statistical reliability. Taking the 0.5s delay as a representative example, the comparison of position error curves between the proposed algorithm and the uncompensated delay factor graph (UDFG) algorithm is shown in Fig. 9. In addition, the statistical RMSE of position and the average single-step computation time under different delay conditions are summarised in Table 3.

It can be seen from Fig. 9 that under the 0.5s delay, the position error of the UDFG algorithm exhibits obvious divergence because it does not process the time delay error. Moreover, Fig. 10 and Table 3 indicate that as the delay increases from 0.3s to 0.9s, the position error of the UDFG algorithm increases sharply. In contrast, the DDFG algorithm effectively suppresses the error divergence. Even under the large delay of 0.9s, the algorithm maintains high positioning accuracy. The slight fluctuations observed

https://doi.org/10.1017/aer.2026.10227 Published online by Cambridge University Press

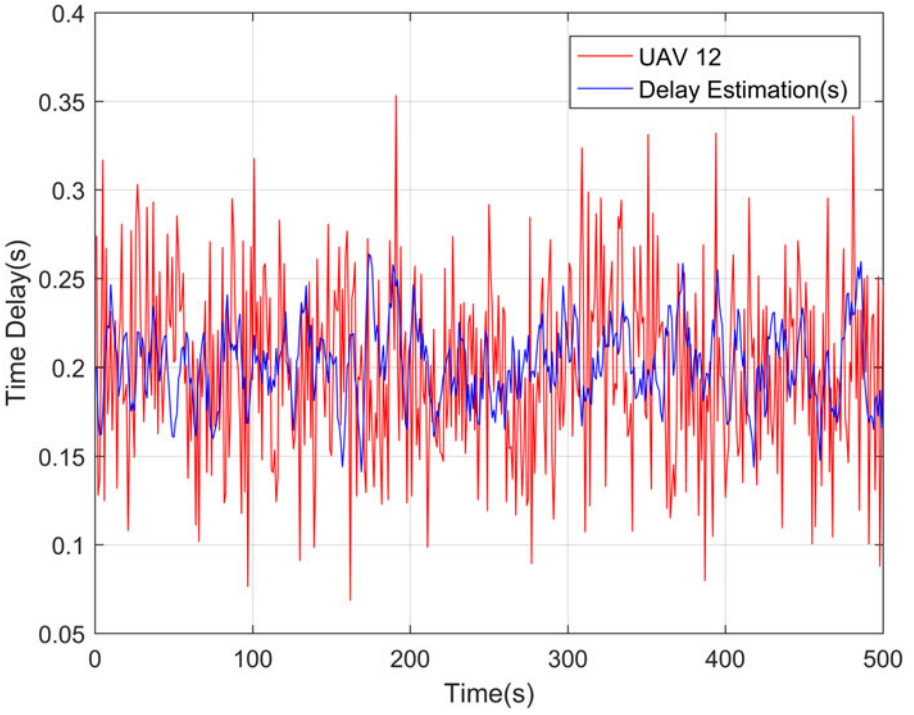


Figure 8. *The comparison between the actual value and the estimated value of UAV12 delay.*

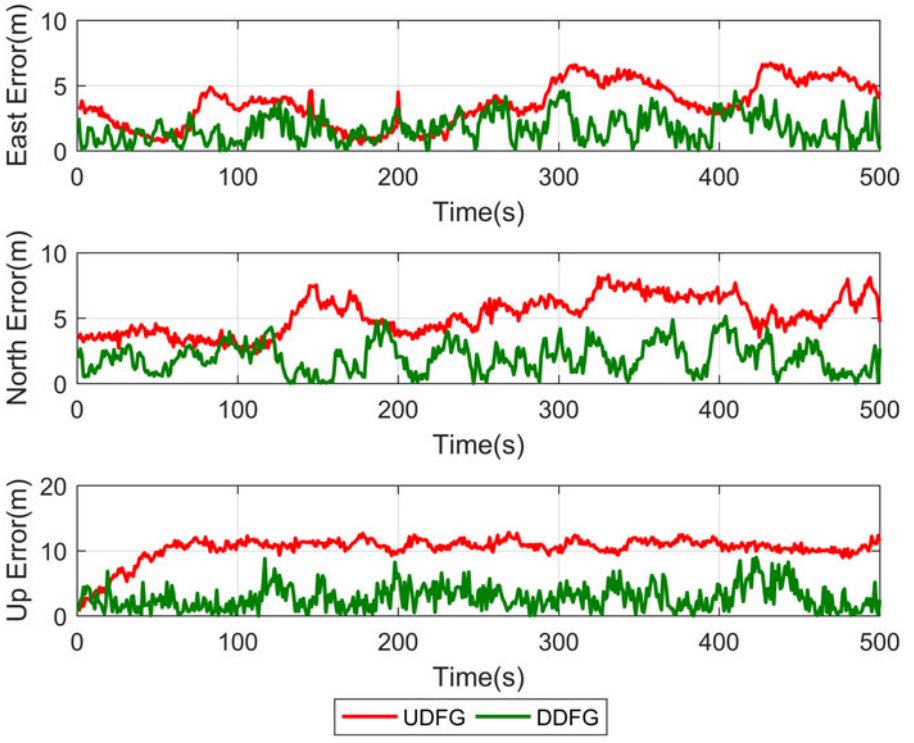


Figure 9. *UAV1 position error (fixed time delay $T = 0.5$).*

https://doi.org/10.1017/aer.2026.10227 Published online by Cambridge University Press

Table 3. *Comparison of position RMSE and calculation time under different delay conditions*

Condition	Algorithm	RMSE of position (m)	Average computation time per update (s)
0.3s ($\sigma = 0.03$)	UDFG	6.63 ± 2.14	0.064
	DDFG	3.67 ± 0.52	0.078
0.5s ($\sigma = 0.05$)	UDFG	9.28 ± 2.96	0.065
	DDFG	4.51 ± 0.67	0.079
0.7s ($\sigma = 0.07$)	UDFG	13.45 ± 3.71	0.065
	DDFG	5.77 ± 0.98	0.080
0.9s ($\sigma = 0.10$)	UDFG	20.90 ± 5.67	0.066
	DDFG	8.02 ± 1.60	0.080

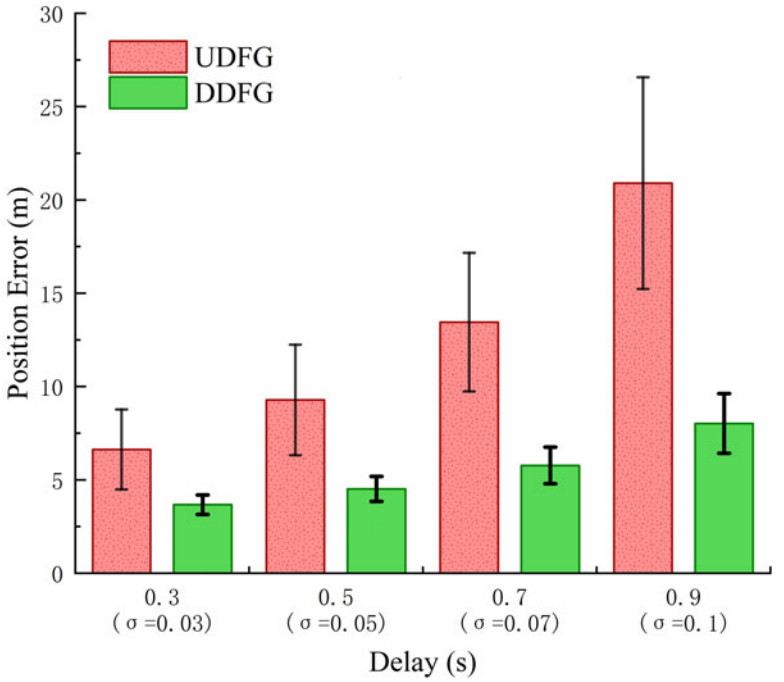


Figure 10. *Statistical comparison of position RMSE (Mean ± SD) for different algorithms under varying communication delays.*

in the DDFG algorithm are due to the fact that as the delay value increases, the EKF processing used for the nonlinear motion equation causes a deviation from the actual motion, affecting the convergence within a fixed number of iterations. Compared with the UDFG algorithm, the proposed algorithm effectively reduces the positioning deviation with only a slightly higher calculation time, and effectively solves the problem of communication delay in cooperative navigation.

4.0 Conclusion

Cooperative navigation of multiple UAVs can improve the positioning accuracy of UAVs, but due to the interaction between UAVs, it will inevitably bring the problem of communication delay. Without

https://doi.org/10.1017/aer.2026.10227 Published online by Cambridge University Press

considering the influence of communication delay, the cooperative navigation algorithm is a sub-optimal algorithm. Therefore, this paper proposes a factor graph distributed data fusion algorithm considering communication delay. The algorithm constructs the delay factor by establishing the UWB propagation delay model and introduces the factor graph. Combined with the sliding window mechanism and the adaptive step size adjustment strategy, the convergence speed and real-time performance are improved, and the distributed optimisation of the factor graph is realised through message iteration to obtain the globally optimal solution. The simulation results show that the algorithm can effectively fuse the UAV measurement information and still has high navigation accuracy in the presence of communication delay.

However, further research and improvements are required for the cooperative navigation of multi-UAV systems in practical implementation. Specifically, although the current work compensates for delays based on a Gaussian distribution model, real-world communication links often exhibit time-varying and non-Gaussian characteristics due to complex environmental interference. Furthermore, as the scale of the UAV swarm increases, balancing the length of the sliding window with computational efficiency becomes a critical challenge. To address these challenges, future work will explore adaptive sliding window strategies and integrate multi-source fusion with machine learning techniques to strictly constrain error propagation in complex environments. UAV formations will fuse multi-sensor data, including visual, IMU and UWB measurements, to realise real-time environmental perception and mapping. Furthermore, machine learning methods will be employed to establish intelligent NLOS error identification and correction models. These improvements aim to realise active identification and precision calibration of complex errors without relying on external anchor points, thereby ensuring the robustness of UAV formation cooperative navigation even in extreme environments with limited satellite signals.

Competing interests. The authors declare no conflict of interest.

References

[1] Ye, X., Song, F., Zhang, Z. and Zeng, Q. A review of small UAV navigation system based on multisource sensor fusion, *IEEE Sens. J.*, 2023, **23**, (17), pp 18926–18948.
[2] Zhou, X., Tang, Z., Wang, N., Yang, C. and Huang, T. A novel state transition algorithm with adaptive fuzzy penalty for multi-constraint UAV path planning, *Expert Syst. Appl.*, 2024, **248**, p 123481.
[3] Wu, Y., Liang, H., Xuan, S. and Zhang, X. Extended state observer based finite-time fault-tolerant formation control for multi-UAVs, *J. Franklin Inst.*, 2024, **361**, (16), p 107158.
[4] Upadhyay, J., Rawat, A. and Deb, D. Multiple drone navigation and formation using selective target tracking-based computer vision, *Electronics*, 2021, **10**, (17), p 2125.
[5] Kartal, Y., Subbarao, K., Gans, N.R., Dogan, A. and Lewis, F. Distributed backstepping based control of multiple UAV formation flight subject to time delays, *IET Control Theory Appl.*, 2020, **14**, (12), pp 1628–1638.
[6] Wang, S., Zhan, X., Zhai, Y., Shen, J. and Wang, H. Performance estimation for Kalman filter based multi-agent cooperative navigation by employing graph theory, *Aerosp. Sci. Technol.*, 2021, **112**, p 106628.
[7] Zhou, Z., Zhang, Z., Peng, X., Li, G., Tao, Y., Wang, L. and Luo, X. Multi-UAV decentralized cooperative navigation method based on memory-fusion, *Acta Aeronautica Astronaut. Sin.*, 2023, **44**, (20), pp 146–158.
[8] Ma, P., Ji, J., Sui, J. and Lei, M. Research on cooperative formation flight control of multi-UAV with communication time delay, 2021 *International Conference on Control Science and Electric Power System (CSEPS)*, 2021, pp 54–58.
[9] Yan, Z., Wang, L., Wang, T., Yang, Z., Chen, T. and Xu, J. Polar cooperative navigation algorithm for multi-unmanned underwater vehicles considering communication delays, *Sensors*, 2018, **18**, (4), p 1044.
[10] Xu, B., Wang, X., Guo, Y., Zhang, J. and Razzaqi, A.A. A novel adaptive filter for cooperative localization under time-varying delay and non-Gaussian noise, *IEEE Trans. Instrum. Meas.*, 2021, **70**, p 9600615.
[11] Zhang, S. and Cao, Y. Cooperative localization approach for multi-robot systems based on state estimation error compensation, *Sensors*, 2019, **19**, (18), p 3842.
[12] Gopalakrishnan, A., Kaisare, N.S. and Narasimhan, S. Incorporating delayed and infrequent measurements in Extended Kalman Filter based nonlinear state estimation, *J. Process Control*, 2011, **21**, (1), pp 119–129.
[13] Zhou, S., Ren, J., Heng, Y., Dong, X. and Li, Q. Distributed cooperative guidance for multi-missile system with time-varying delays and switching topologies, 2020 Chinese Control Conference, 2020, pp 3464–3470.
[14] Xiao, G., Wang, B., Deng, Z., Fu, M. and Ling, Y. An acoustic communication time delays compensation approach for master–slave AUV cooperative navigation, *IEEE Sens. J.*, 2017, **17**, (2), pp 504–513.
[15] Lu, J., Chen, X., Luo, M.X. and Yang, T.F. Cooperative localization algorithm considering of communication delay for autonomous underwater vehicles, *Control Theory Appl.*, 2020, **37**, (9), pp 2061–2072.

https://doi.org/10.1017/aer.2026.10227 Published online by Cambridge University Press

[16] Yang, H., Li, H., Xia, Y. and Li, L. Distributed Kalman filtering over sensor networks with transmission delays, *IEEE Trans. Cybern.*, 2021, **51**, (11), pp 5511–5521.
[17] Cai, W., Liu, Z., Zhang, M., Lv, S. and Wang, C. Cooperative formation control for multiple AUVs with intermittent underwater acoustic communication in IoUT, *IEEE Internet Things J.*, 2023, **10**, (17), pp 15301–15313.
[18] Huang, H., Li, Q., Huang, Y. et al. A communication delay error compensation algorithm for AUV cooperative navigation based on factor graph, *Unmanned Syst. Technol.*, 2024, **7**, (1), pp 115–123.
[19] Fagundes-Junior, L.A., Coelho, A.F., Villa, D.K.D., Sarcinelli-Filho, M. and Brandao, A.S. Communication delay in UAV missions: a controller gain analysis to improve flight stability, *IEEE Lat. Am. Trans.*, 2023, **21**, (1), pp 7–15.
[20] Du, Z., Qu, X., Shi, J. and Lu, J. Formation control of fixed-wing UAVs with communication delay, *ISA Trans.*, 2024, **146**, pp 154–164.
[21] Pham, T.V., Vu, D.V., Nguyen, D.T. and Dong, N.N. Cooperative path-following control of fixed-wing UAV swarm under communication delay, 2023 *IEEE/AIAA 42nd Digital Avionics Systems Conference (DASC)*, 2023.
[22] Lv, X., Yang, R., Zhang, H., He, W. and Feng, Z. Cooperative performance assessment of UAV formations under communication delay via belief rule base, *J. Franklin Inst.*, 2025, **362**, (16), p 108103.
[23] Loeliger, H.A., Dauwels, J., Hu, J., Korl, S., Ping, L. and Kschischang, F.R. The factor graph approach to model-based signal processing, *Proc. IEEE*, 2007, **95**, (6), pp 1295–1322.
[24] Ta, D.N., Kobilarov, M. and Dellaert, F. A factor graph approach to estimation and model predictive control on unmanned aerial vehicles, 2014 *International Conference on Unmanned Aircraft Systems (ICUAS)*, 2014, pp 181–188.
[25] Yan, Z., Luan, Z., Liu, J. and Xing, W. A cooperative localization method for multiple unmanned underwater vehicles based on improved factor graph, 2023 *IEEE International Conference on Mechatronics and Automation (ICMA)*, 2023, pp 894–899.
[26] Wang, R., Xu, C., Li, R., Duan, S. and Zhang, X. Cooperative localization and mapping based on UWB/IMU fusion using factor graphs, *IEEE Sens. J.*, 2023, **24**, (14), pp 21931–21940.
[27] Wang, H., Hu, L. and Tao, J. Collaborative navigation method based on adaptive time-varying factor graph, *Aeronaut. J.*, 2025, **129**, pp 788–801.
[28] Quan, S., Chen, S., Zhou, Y., Zhao, S., Hu, H. and Zhu, Q. A robust position estimation method in the integrated navigation system via factor graph, *Remote Sens.*, 2024, **16**, (3), p 562.
[29] Yang, P., Ye, G.Y., Shao, C.L., Yang, S.L. and Huang, Z.X. A distributed factor graph model solving method for cooperative localization of UAV swarms, *Meas. Sci. Technol.*, 2025, **36**, (1), p 016326.
[30] Chen, M., Xiong, Z., Liu, J., Wang, R. and Xiong, J. Distributed cooperative navigation method of UAV swarm based on factor graph, *J. Chin. Inertial Technol.*, 2020, **28**, (4), pp 456–461.
[31] Zhao, Z. and Ma, G. Research on the adaptive filtering-collaborative graph optimization navigation method, *Chin. J. Scientific Instrum.*, 2023, **44**, (7), pp 271–281.

Cite this article: Wang H. and Fang T. A collaborative navigation method based on a delay-aware factor graph. *The Aeronautical Journal*, https://doi.org/10.1017/aer.2026.10227

https://doi.org/10.1017/aer.2026.10227 Published online by Cambridge University Press